High-frequency gravity waves and homogeneous ice nucleation in tropical tropopause layer cirrus

Eric J. Jensen, Rei Ueyama, Leonhard Pfister, Theopaul V. Bui, M. Joan Alexander, Aurélien Podglajen, Albert Hertzog, Sarah Woods, R. Paul Lawson, Ji-Eun Kim, et al.

AGU PUBLICATIONS

Geophysical Research Letters

RESEARCH LETTER
10.1002/2016GL069426

Key Points:
- High-frequency waves primarily result in high ice concentrations
- Ice nucleation quenching by high-frequency waves has a minor impact on ice concentrations
- Homogeneous freezing results in ice concentrations exceeding observed values

Correspondence to:
E. J. Jensen,
eric.j.jensen@nasa.gov

Citation:
Jensen, E. J., et al. (2016), High-frequency gravity waves and homogeneous ice nucleation in tropical tropopause layer cirrus, *Geophys. Res. Lett.*, *43*, 6629–6635, doi:10.1002/2016GL069426.

Received 2 MAY 2016
Accepted 6 JUN 2016
Accepted article online 11 JUN 2016
Published online 25 JUN 2016

High-frequency gravity waves and homogeneous ice nucleation in tropical tropopause layer cirrus

Eric J. Jensen[1], Rei Ueyama[1], Leonhard Pfister[1], Theopaul V. Bui[1], M. Joan Alexander[2], Aurélien Podglajen[3], Albert Hertzog[3], Sarah Woods[4], R. Paul Lawson[4], Ji-Eun Kim[5], and Mark R. Schoeberl[6]

[1]NASA Ames Research Center, Moffett Field, California, USA, [2]NorthWest Research Associates, CoRA Office, Boulder, Colorado, USA, [3]Laboratoire de Météorologie Dynamique, CNRS-UMR8539, Institut Pierre Simon Laplace, École Normale Supérieure, École Polytechnique, Universeté Pierre et Marie Curie, Paris, France, [4]Spec, Inc., Boulder, Colorado, USA, [5]NOAA, Boulder, Colorado, USA, [6]Science and Technology Corporation, Columbia, Maryland, USA

Abstract The impact of high-frequency gravity waves on homogeneous-freezing ice nucleation in cold cirrus clouds is examined using parcel model simulations driven by superpressure balloon measurements of temperature variability experienced by air parcels in the tropical tropopause region. We find that the primary influence of high-frequency waves is to generate rapid cooling events that drive production of numerous ice crystals. Quenching of ice nucleation events by temperature tendency reversal in the highest-frequency waves does occasionally produce low ice concentrations, but the overall impact of high-frequency waves is to increase the occurrence of high ice concentrations. The simulated ice concentrations are considerably higher than indicated by in situ measurements of cirrus in the tropical tropopause region. One-dimensional simulations suggest that although sedimentation reduces mean ice concentrations, a discrepancy of about a factor of 3 with observed ice concentrations remains. Reconciliation of numerical simulations with the observed ice concentrations will require inclusion of physical processes such as heterogeneous nucleation and entrainment.

1. Introduction

The importance of atmospheric waves for the production of ice crystals in the upper troposphere stems from the strong sensitivity of ice concentrations produced by homogeneous freezing of aqueous aerosols to cooling rate [*Jensen and Toon*, 1994; *Kärcher and Lohmann*, 2002]. The impact of temperature variability driven by waves on cirrus ice concentration has been investigated in a number of modeling studies [e.g. *Kärcher and Ström*, 2003; *Jensen and Pfister*, 2004; *Hoyle et al.*, 2005]. There has been recent debate about whether the upper tropospheric temperature variability and corresponding model predictions of ice concentrations produced by homogeneous freezing can be reconciled with observed ice concentrations in cold cirrus clouds [*Spichtinger and Krämer*, 2013; *Murphy*, 2014; *Schoeberl et al.*, 2015; *Dinh et al.*, 2016; *Jensen et al.*, 2016a]. In particular, *Spichtinger and Krämer* [2013] and *Dinh et al.* [2016] have argued that quenching of nucleation events by the reversal of temperature tendency in high-frequency waves can explain the relatively low ice concentrations typically observed in cirrus forming in the cold tropical tropopause layer (TTL, ≃13–18 km). We note, however, that *Spichtinger and Krämer* [2013] used an idealized wave spectrum and *Dinh et al.* [2016] did not actually show the impact of high-frequency waves and the quenching process on the statistics of ice concentration. The recent tropical superpressure balloon (SPB) measurements (used in the nucleation simulations presented by *Dinh et al.* [2016]) provide the best information available about the actual temperature variability experienced by TTL air parcels, and thus, these measurements are very useful for driving simulations of the initial stages of cirrus formation. Here we reexamine the role of high-frequency waves in homogeneous-freezing ice nucleation at low temperatures, as well as the consistency between theory and measured ice concentrations, using parcel model simulations driven by the SPB measurements.

2. Physical Processes Affecting Cirrus Ice Concentration

The ice concentrations in the earliest stages of cirrus formation are controlled by ice nucleation processes. Many previous modeling studies have assumed that ice production in clouds colder than about −40°C is dominated by homogeneous freezing of aqueous aerosols. Laboratory measurements suggest that the onset of

homogeneous freezing is independent of the detailed chemical composition of the aqueous aerosols [*Koop et al.*, 2000]; with this simplification, the fraction of aerosols that freeze to produce ice crystals is primarily controlled by cooling rate. However, the accuracies of laboratory measurements do not preclude the possibility of some composition dependence, which could significantly decrease the ice concentrations produced by homogeneous freezing [*Murphy*, 2014].

High-frequency waves tend to increase maximum cooling rates and therefore increase ice concentrations. However, if a nucleation event occurs during the phase of the wave when the temperature tendency changes from cooling to heating, then the ice nucleation will be halted, potentially resulting in relatively low ice concentrations [*Jensen et al.*, 2010; *Spichtinger and Krämer*, 2013]. (*Murphy* [2014] similarly showed that waves can produce both slow cooling and fast cooling events, resulting in a wide range of ice concentrations.) This quenching effect is particularly important for high-frequency waves with periods approaching the duration of nucleation events (the time span from the nucleation of the first ice crystal until the peak ice concentration is reached). *Dinh et al.* [2016] showed that this quenching mechanism does occur some of the time in nucleation simulations driven by the SPB measurements.

The alternative mechanism for formation of ice at low temperatures is heterogeneous nucleation on solid particles, either insoluble inclusions in aqueous aerosols or dry particles. Measurements of residual particles remaining after cirrus ice crystal sublimation suggests that heterogeneous nucleation may play a dominant role in ice production, at least for midlatitude cirrus [*Cziczo et al.*, 2013]. Since the concentration of heterogeneous ice nuclei is generally relatively low, the ice concentrations in cirrus produced by this process will tend to be lower than in cirrus produced by homogeneous freezing. Neither the composition nor abundance of effective ice nuclei in the TTL is currently known. Potential TTL particle types that might be effective as heterogeneous nuclei include mineral dust, effloresced ammonium sulfate [*Abbatt et al.*, 2006], and glassy organic-containing aerosols [*Murray et al.*, 2010; *Wilson et al.*, 2012].

As cirrus ice crystals grow, they quickly start to sediment, effectively dispersing the collection of ice crystals vertically and reducing the ice concentrations. Cirrus fallstreaks produced by ice crystal sedimentation generally have much lower ice concentrations than the upper parts of cirrus where nucleation occurred [*Heymsfield et al.*, 2005]. Modeling studies have shown that inclusion of sedimentation is critical for simulating realistic ice concentrations through the full life cycles of cirrus [*Spichtinger and Gierens*, 2009; *Jensen et al.*, 2012, 2013a; *Murphy*, 2014].

Cirrus radiative heating can drive small-scale convection and turbulence, and the resulting entrainment and dispersion will tend to reduce ice concentrations over time. However, in optically thin cirrus forming in the cold TTL, which is the focus of this study, radiative heating rates are relatively weak. Modeling studies have shown that TTL cirrus must persist on the order of a day or more before radiative destabilization drives significant mixing in the clouds [*Dinh et al.*, 2010; *Jensen et al.*, 2011; *Dinh et al.*, 2014]. Therefore, this process may only affect ice concentrations for relatively long-lived TTL cirrus. Although the TTL is generally thermally stable compared to lower levels in the troposphere, it is a region with strong wind shear, and it is not clear to what degree turbulence and entrainment affects ice concentrations in TTL cirrus.

3. Lagrangian Temperature Variability in the TTL

Addressing the issue of high-frequency wave impacts on ice nucleation is only possible with information about the temperature variability experienced by air parcels. Superpressure balloons drift along isopycnic (constant density) surfaces and thus provide the closest approximation available to parcel temperature variability. We use data from two tropical SPB flights conducted by the French Space Agency as part of the pre-Concordiasi campaign [*Rabier et al.*, 2010]. Several adjustments to the SPB measurements are required to derive temperature time series experienced by TTL air parcels (see *Podglajen et al.* [2016] for details). First, the direct SPB temperature measurements are not used because of noise and radiation errors, and instead, the balloon vertical displacement measurements are used to derive temperature perturbations with an assumption that the displacements are adiabatic. For wave frequencies less than about half the Brunt-Väisälä frequency, isentropic displacements are about 3.3 times larger than the measured isopycnic displacements [*Podglajen et al.*, 2016]. In a Lagrangian frame of reference, temperature perturbations in the uppermost tropical troposphere should be approximately equal to temperature perturbations at the balloon altitude ($\simeq$19 km) in the lowermost stratosphere [*Dinh et al.*, 2016]. The balloon buoyancy oscillations have a frequency of 0.25 min^{-1}, which is near the Brunt-Väisälä frequency in the TTL. A Butterworth band-stop filter is applied to remove the

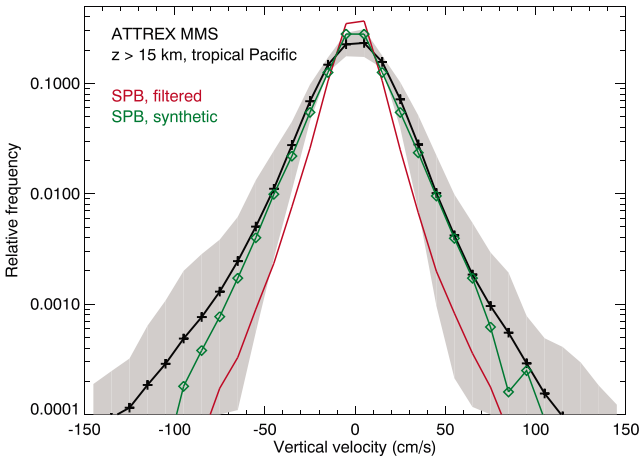

Figure 1. Frequency distributions of vertical wind velocity from the superpressure balloon time series and aircraft measurements. Black curve, mean frequency distribution from ATTREX aircraft measurements in the TTL over the Pacific using the Meteorological Measurement System; grey shading, flight-to-flight range of ATTREX MMS measurements; red curve, filtered balloon data (used in nucleation calculations); green curve, synthetic time series with high-frequency waves added to the filtered balloon data.

balloon neutral oscillations. The total uncertainty in cooling rate estimates from the balloon data is about 2 K h^{-1} [*Podglajen et al.*, 2016].

As a check on the SPB measurements of TTL temperature variability, we compare the SPB vertical wind speeds with aircraft measurements from the Airborne Tropical TRopopause Experiment (ATTREX). (Cooling rate is linearly proportional to vertical wind speed for adiabatic motions.) The Meteorological Measurements System (MMS) [*Scott et al.*, 1990] was used on flights with the NASA Global Hawk unmanned aircraft spanning the tropical Pacific and covering the 14–19 km altitude range [*Jensen et al.*, 2013b, 2016b]. The precision of the MMS vertical wind measurements is 0.05 m s^{-1}. The drift of aircraft properties (e.g., with decreasing fuel load) affect the corrections for aircraft motion and produce long term (0.5 h or more), spurious variations in vertical wind, yielding an accuracy of 0.3 m s^{-1}. These spurious variations can be eliminated by high-pass filtering, which also eliminates real, synoptic-scale variations. However, these are generally small (a few cm s^{-1}). For the small-scale variations most important for the cooling rates, the 0.05 m s^{-1} precision is the applicable uncertainty. Figure 1 shows the frequency distributions of vertical winds from the MMS and SPB measurements. Considerable flight-to-flight variability is evident in the MMS vertical wind speed statistics (grey shading in figure), but the mean distributions using just the eastern or western Pacific measurements are similar to the overall mean distribution shown (black curve). The vertical wind speeds tended to be somewhat larger in the lower TTL (below 15 km) over the highly convective western Pacific than near the tropopause. The MMS measurements give a somewhat broader distribution of vertical wind velocities than the low-pass filtered SPB measurements (red curve) used in the nucleation calculations described below. Also shown is the vertical wind speed distribution from a synthetic time series constructed to match the SPB data at low frequencies and extended to high frequencies (green curve, see *Podglajen et al.* [2016] for details). This vertical wind spectrum agrees well with the MMS observations. We conclude from this comparison that the filtered SPB time series used here certainly does not exaggerate the occurrence of large vertical wind velocities and probably underestimates the width of the vertical wind speed frequency distribution.

Several past modeling studies of TTL wave effects on cirrus and water vapor have used the parameterized wave spectrum derived by *Jensen and Pfister* [2004] (hereafter JP04). This parameterization was developed to represent the typical upper troposphere Lagrangian temperature variability driven by a range of wave types. The temperature adjustment consists of a Fourier series in time with 70 frequencies ranging from 3.2×10^{-7} to 10^{-3} Hz. Wave amplitudes are based on aircraft, radiosonde, and constant-density balloon measurements available at the time. Vertical wavelengths are chosen at random within the 1.5 to 5 km range, and phases for each wave frequency are also chosen at random. Since modern meteorological analyses include waves with frequencies up to 2 cycles d^{-1}, we superimpose only the high-frequency components of the JP04 spectrum on the ERA-interim trajectories for nucleation simulations discussed below. We also use the approach developed by *Kim and Alexander* [2013] (hereafter KA13) to properly interpolate wave amplitudes between the ERA model levels and amplify the wave amplitudes resolved in ERA based on comparisons with radiosondes.

Figure 2 compares the frequency distributions of temperature tendency based on trajectories generated from ERA analysis fields, ERA trajectories with the KA13 interpolation and JP04 wave scheme applied, and the SPB measurements. The ERA trajectories include only relatively long-period waves with cooling rates less than about 4 K h^{-1}. Even with the JP04 parameterization of high-frequency waves applied, the occurrence of rapid cooling rates in the ERA trajectories is considerably underestimated compared to the SPB time series.

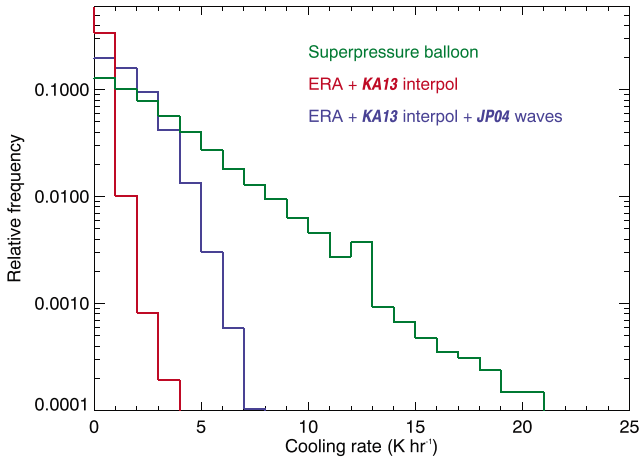

Figure 2. Frequency distributions of cooling rate from parcel temperature time series used for nucleation simulations. Red, ERA-interim trajectory with *Kim and Alexander* [2013] interpolation/amplification scheme applied; blue, ERA trajectory with KA13 scheme applied and JP04 high-frequency waves superimposed; green, SPB time series.

Comparison of temperature perturbation power spectra (not shown) indicates that the potential energy in the JP04 scheme at frequencies larger than 2 cycles d^{-1} is less than half of that in the balloon time series.

4. Ice Nucleation Simulations

4.1. Model Description

Since the SPB measurements only provide temperature time series at a particular vertical level, we focus here on box model simulations of ice nucleation. We use a detailed treatment of ice crystal nucleation and growth, in which hundreds of individual ice crystals are tracked to represent the cloud [*Jensen and Pfister*, 2004]. The activity of aqueous aerosols is assumed to stay in equilibrium with the ambient humidity. This assumption can break down for large (supermicron) aerosols when rapid cooling driven by high-frequency gravity waves occurs [*Haag et al.*, 2003], but under these conditions, ice concentration is dominated by freezing of more numerous, smaller aerosols, so the aerosol activity equilibrium assumption should not affect our results. Water vapor reduction/addition resulting from ice crystal deposition growth/sublimation is accounted for.

We use the time series of temperature perturbations derived from the SPB displacements as input to parcel model simulations of homogeneous-freezing nucleation. In order to provide a large ensemble of realizations, we start the simulations at different times along the SPB time series and with different initial temperatures ranging from 185 to 200 K. Each simulation is initialized with a relative humidity with respect to ice (RHI) of 130%, and we run each simulation until the RHI exceeds the threshold for initiation of homogeneous freezing (RHI $\simeq$ 160–170% at TTL temperatures). Note that the simulated ice concentrations are not sensitive to the initial RHI assumed. We stop each simulation once the ice concentration is sufficiently large such that the RHI is decreasing and will continue decreasing even if the cooling rate suddenly increases. As a result, we are including the "shadowing effect" discussed by *Hoyle et al.* [2005], whereby nucleation of a relatively low number of crystals by weak cooling can limit the ice concentration in a rapid cooling event that immediately follows. Inclusion of sedimentation in parcel model cloud simulations requires assumption about the vertical depth of the parcel. Further, parcel models cannot represent the lower portions of clouds where low ice concentrations are produced by sedimentation from above. The approach used here, which provides only the peak ice concentration just after nucleation, will necessarily give ice concentrations larger than typically observed in TTL cirrus because sedimentation and entrainment would decrease ice concentrations as the clouds age. However, the parcel model simulations are useful for isolating the impacts of high-frequency waves.

In order to represent the effects of sedimentation, we also include 60 day one-dimensional simulations driven by temperature curtains extracted from the ERA fields along diabatic trajectories. (See *Ueyama et al.* [2015] and *Jensen et al.* [2016a], for details of the curtain simulations.) We use a fine vertical grid (0.4 K potential temperature grid resolution), and vertical structure in water vapor concentration driven by cloud processes has an important impact on ice nucleation events downstream of the early cloud events. However, the 1-D simulations do not treat the impacts of wind shear, which is an additional driver of vertical structure in TTL water vapor concentration.

4.2. Simulated Ice Concentrations

Figure 3 shows the frequency distribution of peak ice concentrations produced by these parcel model simulations based on the first of the two SPB temperature perturbation time series (green curve). Results based on the second SPB flight are very similar to those presented here. We also show ice concentrations from parcel model simulations driven by ERA trajectories with the KA13 interpolation applied and with/without JP04

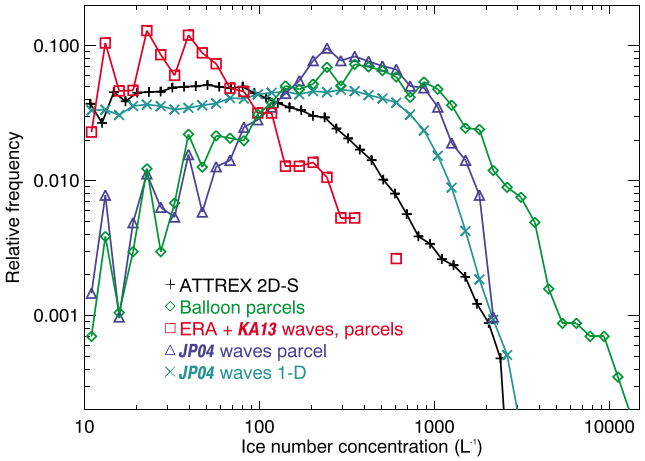

Figure 3. TTL cirrus ice concentration frequency distributions from ATTREX 2D-S measurements (black curve); parcel model simulations using superpressure balloon temperature time series (green curve); parcel model simulations using ERA-interim trajectories with the KA13 wave interpolation/amplification applied (red curve); parcel model simulations with the KA13 scheme applied and the JP04 wave perturbations (blue curve), and one-dimensional simulations using ERA temperature curtains with the KA13 scheme applied and JP04 waves (cyan curve).

high-frequency waves superimposed (red and blue curves, respectively). As expected, higher ice concentrations are produced by the faster cooling events in the SPB time series than in the other simulations. With only the ERA temperature variability, ice concentrations never exceed several hundreds per liter.

Inclusion of sedimentation in the 1-D simulations generally increases the occurrence of low ice concentrations (compare cyan and blue curves). Since the temperature variability included in these 1-D simulations (with high-frequency waves based on the JP04 scheme) is lower than that indicated by the SPB measurements (see Figure 2), the cyan curve should be an underestimate of the ice concentrations predicted by 1-D simulations with homogeneous freezing as the only ice nucleation mechanism.

The frequency distribution of measured TTL cirrus ice crystals from the ATTREX flights is also shown in Figure 3. The ice crystal concentrations are based on measurements from the two-dimensional Stereo (2D-S) probe as part of the Hawkeye instrument [*Lawson et al.*, 2006] flown on the Global Hawk. *Jensen et al.* [2016a] showed that the 2D-S ice concentrations agreed well with those indicated by the Forward Scattering Spectrometer Probe that was also included in the Hawkeye instrument, providing confidence in the measurements. Also, the ATTREX campaign included more than 40 h of measurements in TTL cirrus, and this data set likely provides a reasonable representation of typical TTL cirrus ice concentrations. The occurrence of ice concentrations exceeding 100 L^{-1} is much greater in the homogeneous-freezing simulations presented here than indicated by the ATTREX measurements. As discussed above, the parcel model approach without sedimentation used here necessarily overestimates ice concentrations. However, the ice concentrations simulated using a one-dimensional model with JP04 high-frequency waves still produce higher ice concentrations than those indicated by the observations, and the JP04 parameterization underestimates high-frequency wave amplitudes (Figure 2). The implications of the model/measurement discrepancy are discussed further below.

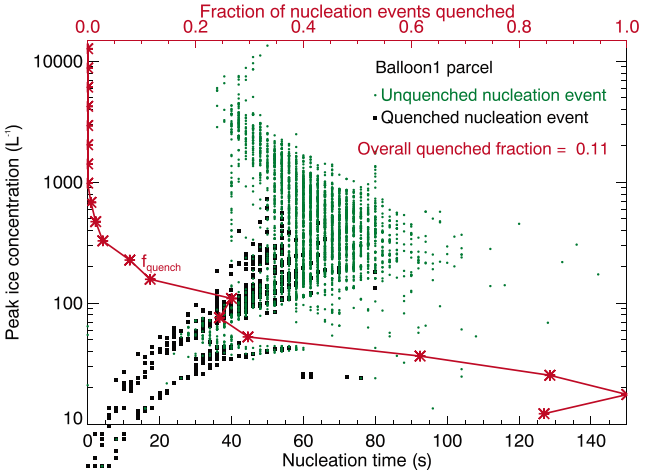

Figure 4. The duration of nucleation events is plotted versus the peak ice concentration produced by homogeneous freezing. Green points, unquenched nucleation events; black squares, quenched nucleation events. (See text for details.) The red curve shows the fraction of nucleation events that are quenched versus peak ice concentration. Overall, 11% of the ice nucleation events are limited by the quenching effect of high-frequency waves.

4.3. Impact of High-Frequency Waves

As discussed above, high-frequency waves tend to provide rapid cooling events that produce large ice concentrations, whereas waves with periods comparable to the nucleation event duration can limit ice concentrations.

In order to quantify the relative importance of the latter effect, we define a nucleation event as "quenched" if the temperature tendency changes from cooling to warming before the maximum ice concentration is reached. Figure 4 shows the time duration of individual nucleation events versus the peak ice concentration, with quenched nucleation events indicated by black squares and unquenched events shown as green points. As expected, the relatively infrequent low ice concentrations produced by homogeneous freezing are typically caused by the quenching effect. However, the quenching process does not prevent the frequent occurrence of ice concentrations greater than a few hundreds per liter nor the occasional occurrence of ice concentrations exceeding 1000 L^{-1}.

As a further test of the net impact of high-frequency waves, we have run parcel simulations with a low-pass filtered version of the SPB temperature perturbation time series such that waves with frequencies greater than 2 cycles h^{-1} are absent. This filtering eliminates cooling rates higher than about 5 K h^{-1}. The resulting ice concentrations (not shown) are restricted to values less than about 400 L^{-1}. From this experiment, we conclude that the overwhelming effect of high-frequency waves is to enhance the occurrence of large ice concentrations produced by homogeneous freezing, and the quenching effect is not sufficient to reduce simulated ice concentrations to observed values.

5. Summary and Discussion

From our parcel model simulations driven by superpressure balloon measurements, we draw the following conclusions:

1. The primary impact of high-frequency temperature variability indicated by the SPB measurements on homogeneous-freezing ice nucleation at low temperatures is to generate frequent occurrences of peak ice concentrations greater than a few hundreds per liter.
2. The quenching effect of very short period waves is significant at reducing ice concentrations in some cases, but overall, this effect does not compensate for the larger cooling rates associated with the high-frequency waves.
3. The peak ice concentrations just after nucleation events predicted by parcel model simulations of homogeneous freezing far exceed the measured ice concentrations in TTL cirrus.

Both *Spichtinger and Krämer* [2013] and *Schoeberl et al.* [2015] showed good agreement between observed ice concentrations and parcel model simulations with ice production by homogeneous freezing. However, both of these studies included sedimentation removal from the parcels, and, as discussed above, this approach does not properly represent the strong vertical gradient in ice concentration produced by sedimentation. Further, *Spichtinger and Krämer* [2013] used an idealized wave specification with only low-frequency and high-frequency oscillations. As discussed above, *Dinh et al.* [2016] showed examples of cases where the quenching effect produced low ice concentrations, and they argued that this mechanism could resolve the discrepancy between ice concentrations predicted by homogeneous freezing and observed ice concentrations. However, they did not show the impact of the quenching effect on ice concentration statistics, nor did they show any comparisons with observed ice concentrations.

One-dimensional simulations (Figure 3) driven by ERAi trajectories including the KA13 interpolation scheme and JP04 high-frequency wave parameterization still overestimate the occurrence of large ice concentrations [*Jensen et al.*, 2016a], and the SPB time series suggest that the JP04 wave scheme is underestimating the high-frequency temperature variability (Figure 2). If we amplify the waves in the JP04 scheme, the resulting distribution of ice concentrations is shifted about a factor of 3 higher than the measured ice concentrations. These comparisons suggest that physical processes other than homogeneous freezing (based on the commonly used *Koop et al.* [2000] parameterization) and sedimentation must be included in numerical simulations to achieve agreement with the observed frequency distributions of ice concentration in TTL cirrus. Likely candidates include heterogeneous ice nucleation on solid or mixed-phase particles, homogeneous-freezing dependence on aerosol composition, and small-scale mixing dilution as the ice clouds age.

Acknowledgments
This work was supported by NASA's Atmospheric Composition Campaign Data Analysis and Modeling program directed by Hal Maring.

References

Abbatt, J. P. D., S. Benz, D. J. Cziczo, Z. Kanji, U. Lohmann, and O. Möhler (2006), Solid ammonium sulfate aerosols as ice nuclei: A pathway for cirrus formation, *Science*, *313*, 1770–1773.

Cziczo, D. J., K. D. Froyd, C. Hoose, E. J. Jensen, M. Diao, M. A. Zondlo, J. B. Smith, C. H. Twohy, and D. M. Murphy (2013), Clarifying the dominant sources and mechanisms of cirrus cloud formation, *Science*, *340*, 1320–1324.

Dinh, T. P., D. R. Durran, and T. Ackerman (2010), Maintenance of tropical tropopause layer cirrus, *J. Geophys. Res.*, *115*, D02104, doi:10.1029/2009JD012735.
Dinh, T. P., S. Fueglistaler, D. R. Durran, and T. Ackerman (2014), Cirrus and water vapor transport in the tropical tropopause layer—Part 2: Roles of ice nucleation and sedimentation, cloud dynamics, and moisture conditions, *Atmos. Chem. Phys.*, *14*, 12,225–12,236.
Dinh, T. P., A. Podglajen, A. Hertzog, B. Legras, and R. Plougonven (2016), Effect of gravity wave temperature fluctuations on homogeneous ice nucleation in the tropical tropopause layer, *Atmos. Chem. Phys.*, *16*, 35–46.
Haag, W., B. Kärcher, S. Schaefers, O. Stetzer, O. Möhler, U. Schurath, M. Krämer, and C. Schiller (2003), Numerical simulations of homogeneous freezing processes in the aerosol chamber AIDA, *Atmos. Chem. Phys.*, *3*, 195–210.
Heymsfield, A. J., D. Winker, and G. van Zadelhoff (2005), Extinction-ice water content-effectie radius algorithms for CALIPSO, *Geophys. Res. Lett.*, *32*, L10807, doi:10.1029/2005GL022742.
Hoyle, C. R., B. P. Luo, and T. Peter (2005), The origin of high ice crystal number densities in cirrus clouds, *J. Atmos. Sci.*, *62*, 2568–2579.
Jensen, E. J., and L. Pfister (2004), Transport and freeze-drying in the tropical tropopause layer, *J. Geophys. Res.*, *109*, D02207, doi:10.1029/2003JD004022.
Jensen, E. J., and O. B. Toon (1994), Ice nucleation in the upper troposphere: Sensitivity to aerosol number density, temperature, and cooling rate, *Geophys. Res. Lett.*, *21*, 2019–2022.
Jensen, E. J., L. Pfister, T.-P. Bui, P. Lawson, and D. Baumgardner (2010), Ice nucleation and cloud microphysical properties in tropical tropopause cirrus, *Atmos. Chem. Phys.*, *10*, 1369–1384.
Jensen, E. J., L. Pfister, and O. B. Toon (2011), Impact of radiative heating, wind shear, temperature variability, and microphysical processes on the structure and evolution of thin cirrus in the tropical tropopause layer, *J. Geophys. Res.*, *116*, D12209, doi:10.1029/2010JD015417.
Jensen, E. J., L. Pfister, and T. P. Bui (2012), Physical processes controlling ice concentrations in cold cirrus near the tropical tropopause, *J. Geophys. Res.*, *117*, D11205, doi:10.1029/2011JD017319.
Jensen, E. J., R. P. Lawson, J. W. Bergman, L. Pfister, T. P. Bui, and C. G. Schmitt (2013a), Physical processes controlling ice concentrations in synoptically forced, midlatitude cirrus, *J. Geophys. Res. Atmos.*, *118*, 5348–5360, doi:10.1002/jgrd.50421.
Jensen, E. J., et al. (2013b), The NASA Airborne Tropical TRopopause EXperiment (ATTREX), *SPARC Newslett.*, *41*, 15–24.
Jensen, E. J., et al. (2016a), On the susceptibility of cold tropical cirrus to ice nuclei abundance, *J. Atmos. Sci.*, *1*, doi:10.11175/JAS-D-15-0274.1, in press.
Jensen, E. J., et al. (2016b), The NASA Airborne Tropical TRopopause EXperiment (ATTREX): High-altitude aircraft measurements in the tropical western Pacific, *Bull. Am. Meteorol. Soc.*, *97*, 10.1175/BAMS–D-14-00263.1, in press.
Kärcher, B., and U. Lohmann (2002), A parameterization of cirrus cloud formation: Homogeneous freezing of supercooled aerosols, *J. Geophys. Res.*, *107*, 4010, doi:10.1029/2001JD000470.
Kärcher, B., and J. Ström (2003), The roles of dynamical variability and aerosols in cirrus cloud formation, *Atmos. Chem. Phys.*, *3*, 823–838.
Kim, J.-E., and M. J. Alexander (2013), A new wave scheme for trajectory simulations of stratospheric water vapor, *Geophys. Res. Lett.*, *40*, 5286–5290, doi:10.1002/grl.50963.
Koop, T., B. Luo, A. Tsias, and T. Peter (2000), Water activity as the determinant for homogeneous ice nucleation in aqueous solutions, *Nature*, *406*, 611–614.
Lawson, R. P., D. O'Connor, P. Zmarzly, K. Weaver, B. A. Baker, Q. Mo, and H. Jonsson (2006), The 2D-S (Stereo) probe: Design and preliminary tests of a new airborne, high-speed, high-resolution imaging probe, *J. Atmos. Ocean. Tech.*, *23*, 1462–1477.
Murphy, D. M. (2014), Rare temperature histories and cirrus ice number density in a parcel and one-dimensional model, *Atmos. Chem. Phys.*, *14*, 13,013–13,022, doi:10.5194/acp-14-13013-2014.
Murray, B. J., et al. (2010), Heterogeneous nucleation of ice particles on glassy aerosols under cirrus conditions, *Nat. Geosci.*, *3*, 233–237.
Podglajen, A., A. Hertzog, R. Plougonven, and B. Legras (2016), Lagrangian temperature and vertical velocity fluctuations due to gravity waves in the lower stratosphere, *Geophys. Res. Lett.*, *43*, 3543–3553, doi:10.1002/2016GL068148.
Rabier, F., et al. (2010), The Concordiasi project in Antarctica, *Bull. Am. Meteorol. Soc.*, *91*, 69–86.
Schoeberl, M., E. J. Jensen, and S. Woods (2015), Gravity waves amplify upper tropospheric dehydration, *Earth. Syst. Sci.*, *2*, 485–500.
Scott, S. G., T. P. Bui, K. R. Chan, and S. W. Bowen (1990), The meteorological measurement system on the NASA ER-2 aircraft, *J. Atmos. Ocean. Tech.*, *7*, 525–540.
Spichtinger, P., and K. Gierens (2009), Modelling of cirrus clouds—Part 1b: Structuring cirrus clouds by dynamics, *Atmos. Chem. Phys.*, *9*, 707–719.
Spichtinger, P., and M. Krämer (2013), Tropical tropopause ice clouds: A dynamic approach to the mystery of low crystal numbers, *Atmos. Chem. Phys.*, *13*, 9801–9818.
Ueyama, R., E. J. Jensen, L. Pfister, and J.-E. Kim (2015), Dynamical, convective, and microphysical control on wintertime distributions of water vapor and clouds in the tropical tropopause layer, *J. Geophys. Res. Atmos.*, *120*, 10,483–10,500, doi:10.1002/2015JD023318.
Wilson, T. W., et al. (2012), Glassy aerosols with a range of compositions nucleate ice heterogeneously at cirrus temperatures, *Atmos. Chem. Phys.*, *12*, 8611–8632.